Chapter 2

Materials and Methods

In this chapter, two distinct types of non-edible oil as base fluids, namely castor oil (CO) and engine oil (EO), were chosen for the formation of nano-fluids which was aimed here to improve the flow and thermal properties through the incorporation of nano-additives. The properties of these base fluids, CO and EO as materials have been comprehensively elucidated. Various characterization techniques have been employed to assess morphological profile & chemical composition of nano-additives. Furthermore, detailed discussions on the instrumentation utilized for rheological analysis and thermal conductivity measurements have been provided, facilitating the investigation of flow and thermal behaviour in both base fluids and nano-fluids. Additionally, thorough insights into the synthesis and processing instruments have been provided, ensuring a comprehensive understanding of the experimental procedures employed in present study.

The results of the literature review (in Chapter 1) served as a guide for selecting base oils, namely CO and EO, for the development of nano-fluids to investigate their flow and thermal properties for better lubricating applications.

2.1: Base Oils

2.1.1: Castor Oil (CO)

Ricinus communis, commonly known as castor, is an annual oil seed crop. It belongs to the spurge family euphorbiaceae and thrives in various geographical areas. The castor plant, which can grow as a large shrub or tree depending on the climate, is fast-growing in the wild, reaching heights of up to 12 meters. However, it typically remains smaller when cultivated in temperate zones. Castor beans are primarily cultivated for their seeds, which yield a viscous, pale yellow, non-volatile, and non-drying CO. India is known for their production of castor and specifically state of Gujarat is hub of such farming [1-3].

To extract CO from locally purchased castor beans, the cold press method was employed. The castor beans were first thoroughly cleaned and dried to remove any dirt or debris. Then, the beans were ground into a fine powder using a grinder, increasing the surface area for better oil extraction. The castor bean powder was placed in a clean screw cold press (local vendor), set to operate at low temperatures, preferably below 60°C, to maintain the oil quality. Gradual pressure was applied to the castor bean powder in the press, squeezing out the oil while leaving behind solid residue. The extracted CO was collected as it dripped or flowed out of the press and transferred to clean containers for

storage. After extraction, the CO was filtered to remove any remaining impurities or solid particles. Finally, the filtered CO was stored in clean, airtight glass containers in a cool, dark place away from direct sunlight to maintain its freshness and quality [4]. Typical CO cold press extraction method used here is illustrated in Fig. 2.1.

Fig. 2.1: Typical procedure for castor oil (CO) extraction by cold press method.

2.1.1.1: Properties of CO

The chemical and physical properties of extracted CO have been measured using the standard methods and listed in Table 2.1.

Table 2.1: Properties of CO.

Property	Value
Appearance	Yellow coloured viscous liquid
Specific gravity (at 25°C)	0.960
Hydroxyl number (mg KOH/gm of oil)	162
Saponification value	178.18
Iodine number	83.11
Acid value (mg KOH/gm of oil)	0.15
Kinematic viscosity (at 100°C), mm^2/s	17.3
Kinematic viscosity (at 40°C), mm^2/s	208.9
Viscosity index	88

2.1.1.2: Specific gravity measurement

The ***specific gravity*** of CO at 25°C refers to its density relative to that of water at the same temperature.

The specific gravity of the oil was determined using a density bottle. Initially, a clean and dry stoppered bottle with a capacity of 25 mL was weighed (W0). Subsequently,

the bottle was filled with the CO, and its weight was recorded as (W1). After cleaning and drying the bottle, it was refilled with distilled water, and the weight was measured again, denoted as (W2). The specific gravity of CO was determined by expression:

$$Specific\ gravity = \frac{W1-W2}{W2-W0} \quad \text{.....Eq. (2.1)}$$

Where,

W0 = weight of dry empty density bottle,

W1 = weight of density bottle + oil, and

W2 = weight of density bottle + distilled water.

A ***specific gravity*** of 0.960 measured for CO in the present study indicates that CO is slightly less dense than water [5, 6].

2.1.1.3: Hydroxyl number measurement

The ***hydroxyl number*** gives information about the degree of esterification within the CO sample.

It was determined in the laboratory using ASTM D1957 standard method. A precise amount of CO ranging from 0.5 to 3.0 grams was weighed into the acetylation flask. Using a 10 mL burette, 5 mL of the pyridine-acetic anhydride mixture were carefully measured and added dropwise into the flask. It was ensured that no time was allowed for drainage during this addition. Prior to attaching the condenser, the neck of the flask was moistened with pyridine to create a seal, which was maintained throughout the acetylation process. The CO and acetylating agent were thoroughly mixed by vigorous shaking. The contents were heated on a water bath under reflux condenser for 60 minutes. After cooling the flask to approximately 50°C, 5 mL of distilled water were added from the top of the condenser with a rotary motion to wash the condenser tube. The mixture was then shaken well and gently boiled for 5 to 10 minutes, with intermittent shaking of the flask. After cooling to room temperature, the condenser was detached and washed with 30 mL of butyl alcohol, while the neck, mouth of the flask, and tip of the condenser were further washed with an additional 20 mL of butyl alcohol. If the contents of the flask were not homogeneous, additional butyl alcohol was added until homogeneity was achieved. The free acetic acid was titrated with an alcoholic 0.35 N potassium hydroxide (KOH) solution in the presence of a few drops of phenolphthalein as an indicator. Similar operations were

conducted using 5 mL of pyridine acetic anhydride mixture alone, as well as with a corresponding weight of the CO plus 5 ml of pyridine. The hydroxyl value was calculated using the formula:

$$Hydroxyl\ number = \frac{Y \times N \times 56.1}{m} \quad \text{.....Eq. (2.2)}$$

Where,

Y = volume of KOH solution in ml corresponding to the amount of acetylated CO formed = a + b – c.

where,

a = the volumes in ml of KOH required by blank with pyridine-acetic anhydride mixture,

b = oil plus pyridine, and

c = oil plus pyridine and acetic anhydride,

N = Normality of the KOH solution, and

m = mass of the CO sample.

Finally, the ***hydroxyl number*** was measured 162 mg KOH/g. This signifies the concentration of hydroxyl (-OH) groups present in the CO. These hydroxyl groups make CO highly reactive in various chemical reactions, including esterification and polymerization [7-9].

2.1.1.4: Saponification value measurement

The ***saponification value*** represents the amount of potassium hydroxide (KOH) required to saponify one gram of the oil. This value is indicative of the average molecular weight of the fatty acids present in the oil and can provide insights into its potential for soap-making and other industrial applications.

For measuring ***saponification value,*** 1 gram sample of the CO was weighed into a 250 mL glass conical flask. Subsequently, 10 mL of an iso propyl alcohol-ether mixture (2:1) was added to the flask, followed by the addition of 25 mL of 0.5 N alcoholic KOH. The flask was then connected to a reflux condenser and subjected to reflux using a water bath for 30 minutes, with intermittent shaking. After heating, 3-4 drops of phenolphthalein indicator were introduced to the warm solution, which was then titrated against 0.5 M HCl until reaching the end point. This procedure was repeated for other samples and a blank. The expression for saponification value (S.V) is represented by the equation:

$$Saponification\ value = \frac{(B-S)\times N\times 56.1}{m} \quad \text{.....Eq. (2.3)}$$

Where,

B = Volume of the solution used for the blank titration,

S = Volume of the solution used for determination,

N = Normality of the HCl used, and

M = Mass of the CO sample.

The measured high ***saponification value*** of 175.31 for CO in present study indicates that the CO has the potential to be used in the oil baes applications. As higher saponification value indicates a lower molecular weight of the triglyceride, whereas a lower saponification value suggests a higher molecular weight.

2.1.1.5: Iodine value measurement

The ***iodine value*** is a measure of the amount of unsaturation in a substance, particularly in fats and oils. It indicates the number of double bonds present in the fatty acid chains of the substance. A higher iodine value suggests a greater degree of unsaturation, meaning more double bonds are present, while a lower iodine value indicates less unsaturation and fewer double bonds. This parameter is significant in determining the oxidative stability, nutritional quality, and suitability for various industrial applications of fats and oils.

For measuring iodine value, in a 250 mL conical flask, 0.25 g of CO sample was placed, followed by addition of 10 mL of chloroform and 30 mL of Hanus iodine solution. The flask was securely closed, and the solution was left to shake for 30 minutes in the dark. Subsequently, 10 mL of 15% potassium iodide (KI) solution was added and shaken, after which 100 mL of distilled water was introduced. The resulting mixture was titrated with iodine solution against 0.1 N sodium thiosulfate ($Na_2S_2O_3$) solution until a yellow colour formed. Upon the formation of the yellow colour, 2-3 drops of starch solution were added, resulting in the formation of a blue solution. The titration proceeded until the blue colour disappeared, and the volume of $Na_2S_2O_3$ at the end point was recorded. The iodine value was then calculated according to the method reported by other researchers [10, 11].

$$Iodine\ value = \frac{(V1-V2)\times c\times 12.69}{m} \quad \text{.....Eq. (2.4)}$$

Where,

V1 = Volume of $Na_2S_2O_3$ used for the blank,

V2 = Volume of $Na_2S_2O_3$ used for sample,

c = Concentration of $Na_2S_2O_3$, and

m = mass of the CO sample.

The ***iodine number*** of CO was found 83.11, which indicates level of unsaturation or presence of double bonds in the fatty acid chains of the oil. since CO iodine value is lower than 100. Certainly, the CO could be used extensively as lubricants and hydraulic brake fluids [12].

2.1.1.6: Acid value measurement

Acid value represents the amount of KOH required to neutralize the free fatty acids present in one gram of the oil.

For measuring acid value of CO, in a dried 250 mL conical flask, 5.0 g of the CO sample was placed, followed by the addition of 25 mL of absolute iso-propyl alcohol and 3 drops of phenolphthalein indicator. The mixture was heated in a shaking water bath for 5 minutes. While hot, it was titrated against 0.1 N KOH until a pink colour appeared. Vigorous shaking was performed as the end point was approached to ensure thorough mixing. The volume of 0.1 N KOH consumed by the acid was recorded. Subsequently, acid value was determined based on method described in the literature [11, 13].

$$Acid\ value = \frac{V \times N \times 56.1}{m} \quad \text{.....Eq. (2.5)}$$

Where,

V = Volume of KOH solution,

N = Normality of KOH solution, and

m = mass of CO sample

Here, the measured lower ***acid value*** of CO, expressed as 0.15 mg KOH/g of oil, indicates a lower concentration of free fatty acids, which is desirable for quality and stability.

2.1.1.7: Viscosity measurement

Viscosity index (VI) of an oil is measure of resistance to change in viscosity with temperature variations. It quantifies how the viscosity of the oil varies as the temperature changes, indicating its ability to maintain consistent flow properties across different operating temperatures [14]. ***Kinematic viscosity***, a key parameter in viscosity index determination, indicates oil's resistance to flow under influence of gravity at a specific temperature. The viscosity index is significant because it provides insights into the oil's

performance under varying temperature conditions, particularly in lubrication and hydraulic systems. A higher viscosity index suggests that the oil's viscosity changes less with temperature, indicating better lubricating properties and stability over a wide temperature range. Conversely, a lower viscosity index indicates greater sensitivity to temperature changes, potentially leading to inadequate lubrication and increased wear under extreme operating conditions.

The viscosity index of CO was typically determined according to standardized methods such as ASTM D2270 by using glass viscometers, where the CO sample's kinematic viscosity was measured at specific temperatures (at 100ºC and 40ºC), and the viscosity index is determined in comparison with a reference oil with a known viscosity index. The ***kinematic viscosity*** of the CO at 100ºC and 40ºC was recorded as 208.9 mm^2/s and 17.3 mm^2/s respectively. Based on kinematic viscosities at different temperatures, the ***viscosity index*** of CO was measured 88 [12, 15].

Overall, CO was characterized by its unique combination of chemical and physical properties, making it suitable for various industrial lubricant, pharmaceutical, and cosmetic applications. Its viscosity, lubricating properties, and biodegradability make it particularly useful in industries ranging from cosmetics to automobiles.

2.1.2: Engine Oil (EO)

The EO of 10W-30, 4-AT grade (Fig. 2.2) was obtained from local commercial vendor of Castrol make. The 10W-30, 4-AT grade EO is formulated to meet specific performance requirements in automotive applications. The "10W-30" designation indicates the oil's viscosity characteristics, with "10W" representing its viscosity in cold temperatures and "30" indicating its viscosity at operating temperatures. This grade offers a balanced viscosity profile, providing sufficient lubrication during cold starts while maintaining optimal lubricating properties at higher temperatures. The "4-AT" designation signifies its compatibility with automatic transmission systems, ensuring smooth shifting and efficient power transfer. Overall, the 10W-30, 4-AT grade EO is engineered to deliver reliable performance and protection for modern automotive engines and transmissions [16, 17].

The EO appears as a yellow-coloured viscous liquid, indicating its fluid nature and distinct coloration characteristic of lubricating oils. All the properties measured here as per procedure mentioned in the CO section.

Fig. 2.2: Castrol engine oil (EO), 10W-30, 4-AT grade.

2.1.2.1: Measurements of EO properties

The properties of EO were measured and displayed in Table 2.2.

Table 2.2: Properties of EO.

Property	Value
Appearance	Yellow coloured viscous liquid
Specific gravity (at 25°C)	0.866
Acid value (mg KOH/gm of oil)	0.21
Kinematic viscosity (at 100°C), mm^2/s	11
Kinematic viscosity (at 40°C), mm^2/s	72
Viscosity index	143

The ***specific gravity*** of the EO at 25ºC was measured 0.866 as per procedure mentioned in castor oil section. This value denotes the density of the oil compared to that of water, suggesting that the EO is less dense than water. The ***acid value*** of EO was measured as 0.21 mg KOH/g of oil, indicates a lower concentration of acids, which is desirable for quality and stability of EO. The ***kinematic viscosity*** of the EO at 100ºC and 40ºC was recorded as 11 mm^2/s and 72 mm^2/s respectively. Based on kinematic viscosities at different temperatures, the ***viscosity index*** of EO was measured 143. A higher viscosity index suggests that the oil maintains its viscosity more effectively across a range of temperatures.

In summary, the EO 10W-30, 4-AT grade exhibits specific chemical and physical properties crucial for its function as a lubricating fluid in automotive engines. These properties, including viscosity, density, and alkalinity, contribute to its ability to protect engine components, minimize wear, and ascertain optimal performance in multiple operating conditions.

2.2: Methods used for characterization of nano-additives/ nanofluids

2.2.1: X-Ray Diffraction (XRD) Analysis

X-ray, discovered by Wilhelm Roentgen in 1895, constitutes a short wavelength portion of the electromagnetic spectrum ranging from 10 picometers to 10 nanometres [18-20]. XRD technique serves as a fundamental characterization tool for solids, enabling the determination of their crystal structure, including lattice constants and geometry, as well as the identification of unknown materials and the orientation of single crystals, defects, and crystallite size of nanoparticles.

The X-ray diffraction patterns are acquired by measuring the angles at which an X-ray beam is diffracted by the crystalline phases present in the material. Bragg's equation (Eq. 2.6) establishes a relationship between the distance between two h, k, l planes (d) and the angle of diffraction (2θ)[21].

$$\lambda = 2\, d_{h,k,l}\, Sin\theta \quad \text{.....Eq. (2.6)}$$

Where,

λ = wavelength of the incident radiation, and

θ = Bragg's angle.

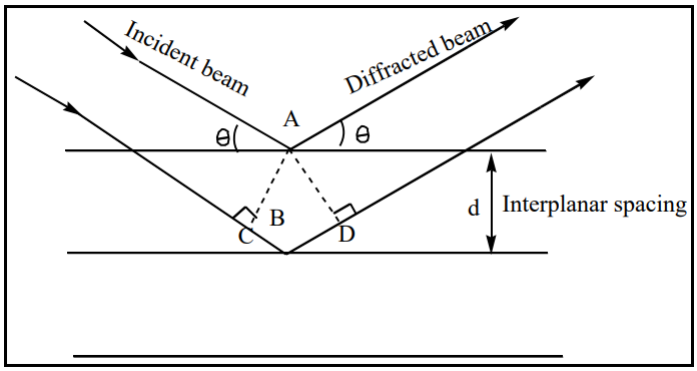

Fig. 2.3: X-rays diffraction by crystal planes.

Additionally, XRD facilitates the calculation of crystallite size using the Scherer formula (Eq. 2.7), which considers parameters such as the wavelength of the X-ray source (λ= 1.5418 Å), the peak width of the diffraction peak profile at full width at half maximum-FWHM (β) resulting from small crystallite size in radians, and the Bragg's angle (θ) [22].

$$D = \frac{0.9\lambda}{\beta cos\theta} \quad \text{.....Eq. (2.7)}$$

In present study, XRD spectra were obtained using a BRUKERAXS GMBH D8 advance X-ray diffractometer (Fig. 2.4) at a scan rate of 0.05 degree/second, employing Cu-kα_1 radiation (1.5406 Å, 40 kV, 40 mA). Here, the crystallite size of nano-additives was calculated using the known Scherer formula and XRD plot compared with ICDD database for phase identification.

Fig. 2.4: X-ray diffractometer.

2.2.2: Scanning Electron Microscopy (SEM)/ Energy Dispersive Spectroscopy (EDS) Analysis

SEM is facilitated by the two pairs of electromagnetic coils situated within the objective lens. One pair directs the beam in the x-direction across the sample, while the other pair controls movement in the y-direction. This scanning process is orchestrated by applying electrical signals to the x coils, causing the electron beam to traverse the sample in a linear fashion. After completing a line scan, the y coils slightly deflect the beam, enabling repeated scanning with the x coils. This rapid movement ensures irradiation of the entire sample surface. The image of the sample is produced by using the output of a detector. Conductive samples are more straightforward to analyse; however, non-conducting samples require the application of metallic films, typically generated through sputtering with metals such as gold, palladium, or platinum, to enhance conductivity for SEM analysis.

In our study, the morphology of nano-additives was examined using a SEM (JEOL JSM 6380LV) equipped with EDX (OXFORD X-ACT SDD). Samples were affixed to SEM stubs using double-sided carbon tape and coated with a thin layer of gold to enhance conductivity. Gold coating was conducted by using JEOL JFC-1600 auto fine coater. Imaging was conducted at various magnification at 15 to 20 kV voltage range, with a working distance of approximately 12 mm. Additionally, an EDX, was employed to assess the morphology and elemental composition present in synthesized nano-additives.

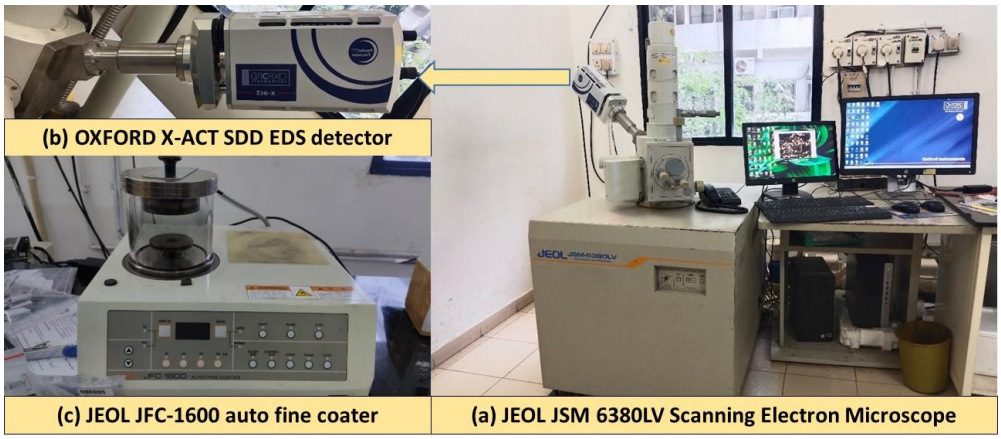

Fig. 2.5: (a) Scanning Electron Microscope (SEM), (b) EDX detector, and (c) auto fine coater.

2.2.3: Rheology measurements

The experimental tests designed to describe and analyse the rheological properties of the different nanofluids were developed by a HAAKE MARS III rheometer (Thermo Scientific), coupled with a parallel plate P25 CS L geometry and a temperature controlling peltier system that ensured the establishment of the set temperature with a 0.1°C accuracy. The rheology software HAAKE RheoWin3 was used to calibrate the instrument. The selected geometry was composed of two parallel plates, which had a 25 mm diameter. Sample was placed on the measuring base plate; and a stainless-steel cover appropriate for avoiding evaporation at high analysing temperatures. The expanded uncertainty (k = 2) of the dynamic viscosity data by using this device was declared to be lower than 5.0% [23, 24].

Rotational tests, find out the fluid behaviour through viscosity vs. shear rate plots once reached the steady state for rheology analysis, were performed for the base fluid and designed nanofluids of varied mass fraction having shear rates between 1 and 5000 s^{-1}, and with temperature ranging from 40°C to 100°C.

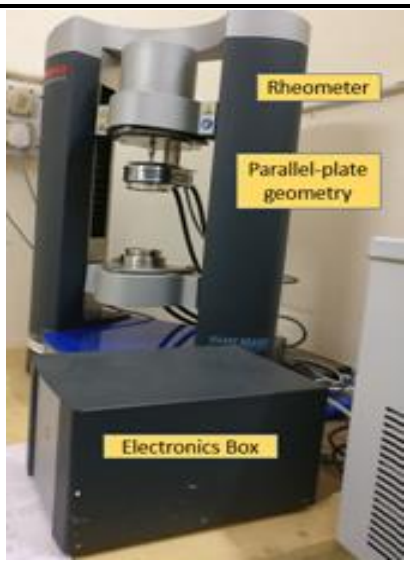

Fig. 2.6: Rheometer.

2.2.4: Thermal conductivity measurements

The characteristic responsible for the transmission of heat within a material is termed as ***thermal conductivity***.

In contemporary mechanical systems, lubricants fulfil a dual function: mitigating friction between moving components to minimize mechanical degradation, and managing thermal conditions by dissipating heat generated during frictional processes. Heat dissipation can occur via thermal conduction or thermal convection, depending on the specific device, although thermal conduction typically prevails in numerous applications. Thermal conductivity of lubricants emerges as a crucial parameter governing their performance.

Fourier's law of heat conduction used to describe the steady-state heat transfer in matter [25]:

$$q = -k\frac{dT}{dx} \quad \text{.....Eq. (2.8)}$$

Where,

q = Heat flux,

x = Thickness,

$\frac{dT}{dx}$ = Temperature gradient, and

k = Proportionality constant i.e. '***Thermal conductivity***'.

The thermal conductivity of the BO and the synthesized nanofluids was evaluated using the C-Therm thermal conductivity apparatus following the ASTM D7984 standard.

This thermal conductivity apparatus, depicted in Fig. 2.7, operates based on the modified transient plane source (MTPS) technique. It comprises a sensor, control electronics, and a data monitoring system.

The sensor utilized for measuring the fluid's thermal conductivity was positioned within an oven to record thermal conductivity across various temperatures. This sensor incorporates a spiral heating element surrounded by a guard ring. Alongside the central spiral heater, the guard ring also emits heat to simulate one-dimensional heat flow from the sensor to the test material in contact. The output signal from the sensor was interfaced with the control electronics for data acquisition and processing. The following steps were adhered to for each measurement:

1. Ensure cleanliness and dryness of the sensor surface.
2. Dispense approximately 1.25 mL of the fluid into the test cell, ensuring the absence of trapped air bubbles near the sensor's surface.
3. Equalize the temperature by placing the test kit in the thermal chamber.
4. Verify the stability of the sensor temperature, with variations not exceeding ±0.1 °C.
5. Perform five consecutive thermal conductivity measurements. Here, each sampling time, allow the sensor and specimen to cool down automatically for 60 seconds.
6. Calculate the average value of thermal conductivity (k).

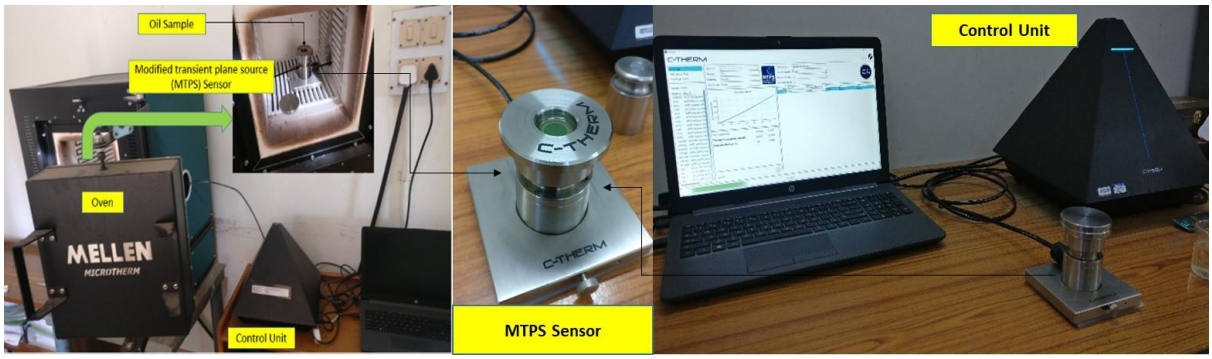

Fig. 2.7: Thermal conductivity meter with modified transient plane source (MTPS).

2.3: Instruments/equipments used to synthesize nano-additives and nanofluids

In this section, the instruments used to synthesize nanomaterials and nanofluids are discussed in detail, providing insight into their individual purposes. Various instruments include the hydrothermal reactor, probe sonicator, analytical balance, pH meter, air circulating oven, and vacuum oven are discussed. Each instrument plays a crucial role in ensuring the accuracy, reproducibility, and success of the experimental procedures. The specifications, operation, and relevance of these instruments were elaborated, providing complete insights into their contributions to the synthesis of nano-additives and nano-fluids.

2.3.1: Hydrothermal reactor

The hydrothermal reactor plays a pivotal role in facilitating the synthesis and processing of materials in various fields, including chemistry, materials science, and nanotechnology. Specifically, the utilization of a 50 mL hydrothermal reactor with a shell made of high-quality nonmagnetic 316 stainless steel (SS) construction and PTFE closing arrangement, as illustrated in Fig. 2.8, offers a controlled and high-pressure environment for conducting hydrothermal reactions. This apparatus enables the synthesis of nanomaterials, such as nanoparticles and nanocomposites, under conditions of elevated temperature (≤240°C) and pressure (≤3MPa), leading to unique structural and morphological properties. In addition to nanomaterial synthesis, the hydrothermal reactor is instrumental in the fabrication of nano-additives, enhancing the functionality and performance of materials [26]. In our experimental setup, the 50ml hydrothermal reactor serves as a crucial tool for nano-additives synthesis, enabling the investigation of their performance in desired applications.

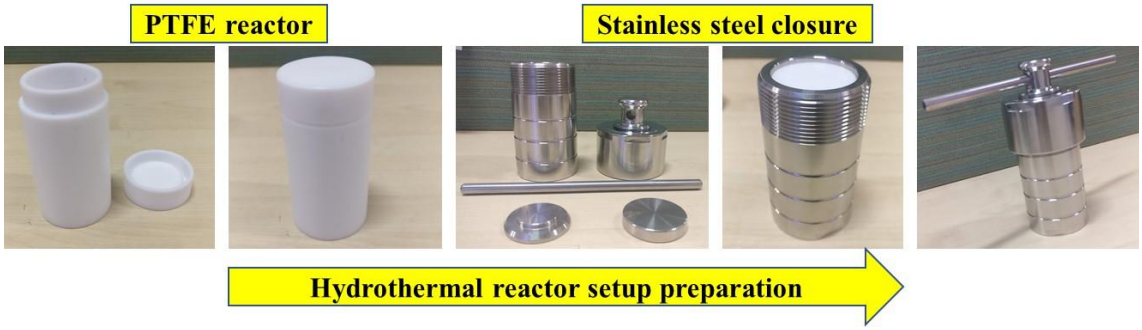

Fig. 2.8: Hydrothermal reactor setup preparation arrangement.

2.3.2: Probe sonicator

The probe sonicator, a critical equipment in nanofluid preparation, utilizes acoustic cavitation to disperse and homogenize nanoparticles within a fluid medium. The Leela Sonic high-power ultrasonication probe, boasting a 500-watt output power and operating at a frequency of 20 kHz, stands out for its ability to precisely control the dispersion process. This sophisticated instrumentation, illustrated in Fig. 2.9, comprises a cabinet housing the ultrasonication probe and a controller designed for meticulous monitoring and adjustment of processing parameters, including temperature, time, and pulse. With its programmable controls, this system empowers processing conditions to meet the specific requirements of nanofluid formulations.

The probe sonicator functions based on the principle of acoustic cavitation, wherein high-intensity sound waves induce the formation of cavitation bubbles within the fluid medium. These bubbles undergo rapid collapse under pressure, generating localized heating, shockwaves, and microstreaming. The resultant mechanical forces effectively energize the nanoparticles, facilitating their dispersion and fragmentation of agglomerates into smaller, more uniform particles. This process supports the development of stabilized nanofluids [27].

- Advantages of probe sonicator:
  - Efficient nanoparticle dispersion: The high-power ultrasonication probe ensures thorough dispersion of nanoparticles within the fluid medium, effectively minimizing agglomeration and achieving a uniform distribution throughout the nanofluid.
  - Customizable processing parameters: The probe sonicator's comprehensive monitoring and programmable controls allow for precise adjustment of parameters such as temperature, time, and pulse, enabling researchers to fine-tune the dispersion process to match the specific characteristics of their nanofluid formulations.
  - Reduced processing time: Ultrasonication significantly accelerates the dispersion process, leading to a notable reduction in the time required for nanofluid preparation compared to conventional techniques.
  - Enhanced nanofluid stability: The severe mechanical forces produced during sonication facilitate the breakup of particle aggregates, resulting in nanofluid

formulations characterized by improved thermal and rheological properties, as well as enhanced stability over time.

Fig. 2.9: High-power ultrasonication probe.

2.3.3: Analytical balance

The Mettler Toledo XSR105 analytical balance (Fig. 2.10 (a)), with its precision of ±0.02 mg, plays an important role in nano-additives and nano-fluids preparation. This cutting-edge instrument enables accurate measurements of the weights. By ensuring precise measurements, it allows to control and optimize the composition of nanofluid formulations with precision, leading to enhanced properties and performance. Additionally, the balance facilitates the preparation of precise concentrations of nano-additives, ensuring reproducibility and reliability in experiments.

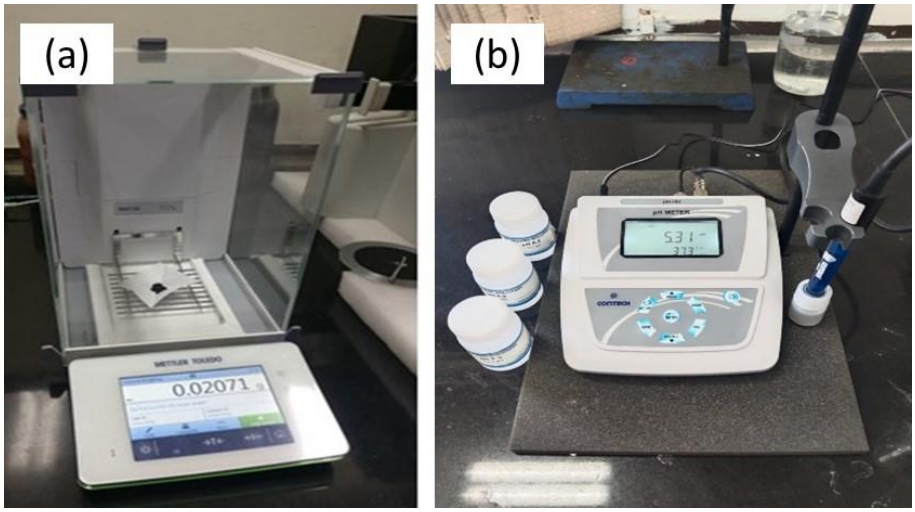

Fig. 2.10: (a) Analytical balance, and (b) pH meter.

2.3.4: pH meter

The Contech pH-2 pH meter is a crucial instrument in the hydrothermal synthesis of nanoparticles, as illustrated in the Fig. 2.10 (b). With its user-friendly interface and reliable performance, this pH meter allows to accurately measure the pH levels of solutions during the synthesis process. It is also calibrated by buffer solutions. These buffer solutions have precisely defined pH values at specific temperatures, typically pH 4.01, pH 7.00, and pH 10.01. Maintaining precise pH conditions is essential for controlling the nucleation and growth of nanoparticles in hydrothermal synthesis. By monitoring and adjusting the pH levels, we can optimize the synthesis conditions to produce nanoparticles with desired size, morphology, and better properties.

2.3.5: Universal Oven

The Memmert UN55 Universal Oven (Fig. 2.11 (a)) was used for exact temperature and time control in hydrothermal synthesis experiments for nano-additive preparation. This oven, constructed of high-quality stainless steel, features superior ventilation and control technologies to provide maximum performance. With a temperature of at least 5°C above ambient to +300°C and a setting precision of up to 0.1°C, it can manage the thermal environment for different experiments. The oven has a digital PID-microprocessor controller with a high-definition TFT-colour display that allows real-time temperature monitoring. The programmable timer, adjustable air flap, and vent connector provide flexibility in experimental setups. Adjustable electronic overtemperature monitoring and mechanical temperature limits are among the safety features that ensure consistent and safe operation.

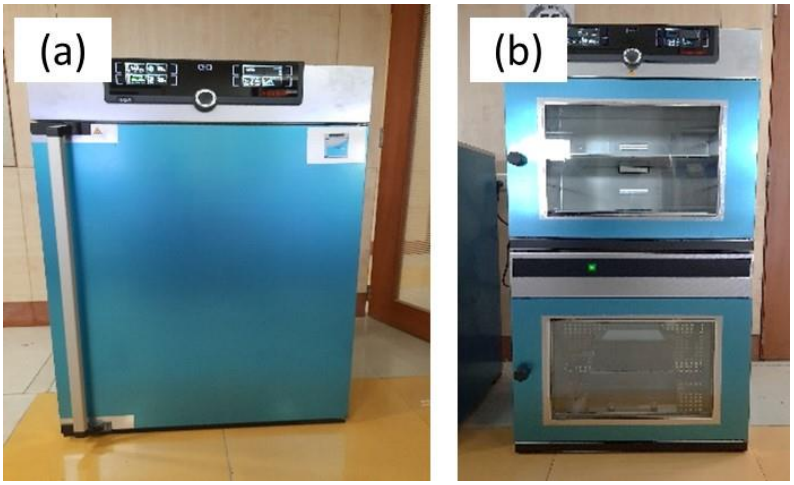

Fig. 2.11: (a) Universal Oven, and (b) Vacuum oven.

2.3.6: Vacuum Oven

For vacuum drying, the Memmert VO29 vacuum oven (Fig. 2.11 (b)) was used. Its direct contact between the load and the heatable and removable thermo-shelves ensures efficient heat transfer without heat loss. With a temperature range from +20 to +200°C and a setting accuracy of up to 0.1°C. The vacuum range of 5 to 1100 mbar, along with digital electronic pressure control, enables gentle and efficient drying of sensitive materials. The oven features a TwinDISPLAY control system with two high-definition TFT-colour displays, offering intuitive operation and real-time monitoring of temperature and pressure parameters.

2.4: References

[1] A. Yeboah, S. Ying, J. Lu, Y. Xie, H. Amoanimaa-Dede, K. G. A. Boateng, M. Chen, and X. Yin, Castor oil (Ricinus communis): a review on the chemical composition and physicochemical properties, Food Science and Technology, 41 (2020) 399-413.

[2] H. Mutlu, and M. A. Meier, Castor oil as a renewable resource for the chemical industry, European Journal of Lipid Science and Technology, 112 (2010) 10-30.

[3] V. R. Patel, G. G. Dumancas, L. C. K. Viswanath, R. Maples, and B. J. J. Subong, Castor oil: properties, uses, and optimization of processing parameters in commercial production, Lipid Insights, 9 (2016) LPI. S40233.

[4] H. Rani, S. Sharma, and M. Bala, Technologies for extraction of oil from oilseeds and other plant sources in retrospect and prospects: A review, Journal of Food Process Engineering, 44 (2021) 11.

[5] M. G. Kulkarni, and S. B. Sawant, Some physical properties of castor oil esters and hydrogenated castor oil esters, European Journal of Lipid Science and Technology, 105 (2003) 214-218.

[6] M. Auta, Extraction and characterization of drilling fluid from castor oil, International Journal of Innovation and Applied Studies, 3 (2013) 382-387.

[7] F. C. Naughton, Production, chemistry, and commercial applications of various chemicals from castor oil, Journal of the American Oil Chemists' Society, 51 (1974) 65-71.

[8] F. C. Naughton, Castor oil, Kirk-Othmer Encyclopedia of Chemical Technology, (2000).

[9] E. Fernandes, J. Vicente, R. Cruz, M. Nele, É. Nunes, and R. Costa-Félix, A methodology free of pyridine for measuring hydroxyl value in polymers and oils, Polymer Testing, 33 (2014) 16-20.

[10] A. Al-Hamdany, and T. Jihad, Oxidation of some primary and secondary alcohols using pyridinium chlorochromate, Tikrit Journal of Pure Science, 17 (2012).

[11] A. Omari, Q. A. Mgani, and E. B. Mubofu, Fatty acid profile and physico-chemical parameters of castor oils in Tanzania, Green and Sustainable Chemistry, 5 (2015) 154-163.

[12] A. Abdelaziz, I. Elamin, G. Gasmelseed, and B. Abdalla, Extraction, refining and characterization of Sudanese castor seed oil, J. Chem. Engeneering, 2 (2014) 1-4.

[13] M. Kyari, Extraction and characterization of seed oil, International Agrophysics, 22 (2008) 139-142.

[14] S. Verdier, J. A. Coutinho, A. M. Silva, O. F. Alkilde, and J. A. Hansen, A critical approach to viscosity index, Fuel, 88 (2009) 2199-2206.

[15] U. Akpan, A. Jimoh, and A. Mohammed, Extraction, characterization and modification of castor seed oil, Leonardo Journal of Sciences, 8 (2006) 43-52.

[16] A. Roslan, A. S. Ibrahem, and A. Hadi, System identification for experimental analysis of SAE 10W-30 automotive engine oil, 19 (2012) 385.

[17] Viscometer, Rate Capillary, Samuel W. Rein, David L. Alexander, and N. Y. Beacon. "Development of a High Shear. In the relationship between engine oil viscosity and engine performance-part V and part VI: Presented at 1980 SAE Congress and Exposition, Cobo Hall, Detroit MI, 460 (1980) 135.

[18] Mould, R. F. Röntgen and the discovery of X-rays. The British Journal of Radiology 68 (1995) 1145-1176.

[19] R. R. Babic, G. S. Babic, S. R. Babic, and N. R. Babic, 120 years since the discovery of X-Rays/120. Godina od otkrica X-Zraka, Medicinski pregled, 69 (2016) 323-331.

[20] R. F. Mould, Röntgen and the discovery of X-rays, British Journal of Radiology, 68 (2014) 1145-1176.

[21] C. G. Pope, X-ray diffraction and the Bragg equation, Journal of chemical education, 74 (1997) 129.

[22] J. I. Langford, and A. Wilson, Scherrer after sixty years: a survey and some new results in the determination of crystallite size, Journal of applied crystallography, 11 (1978) 102-113.

[23] G. Żyła, and J. Fal, Experimental studies on viscosity, thermal and electrical conductivity of aluminum nitride–ethylene glycol (AlN–EG) nanofluids, Thermochimica Acta, 637 (2016) 11-16.

[24] G. Żyła, J. P. Vallejo, J. Fal, and L. Lugo, Nanodiamonds-Ethylene Glycol nanofluids: Experimental investigation of fundamental physical properties, International Journal of Heat and Mass Transfer, 121 (2018) 1201-1213.

[25] Y. Yener, and S. Kakac, Heat conduction: CRC Press, (2018).

[26] Y. X. Gan, A. H. Jayatissa, Z. Yu, X. Chen, and M. Li, Hydrothermal synthesis of nanomaterials, Journal of Nanomaterials, 2020 (2020) 1-3.

[27] A. Asadi, F. Pourfattah, I. M. Szilágyi, M. Afrand, G. Żyła, H. S. Ahn, S. Wongwises, H. M. Nguyen, A. Arabkoohsar, and O. Mahian, Effect of sonication characteristics on stability, thermophysical properties, and heat transfer of nanofluids: A comprehensive review, Ultrasonics sonochemistry, 58 (2019) 104701.